# Influence of the neck shape for Helmholtz resonators

Jean-François Mercier, Jean-Jacques Marigo and Agnès Maurel

*Poems, ENSTA, Palaiseau, France,*

*LMS, Ecole Polytechnique, Palaiseau, France,*

*Institut Langevin, ESPCI, Paris, France*

## Abstract

The resonance of a Helmholtz resonator is studied with a focus on the influence of the neck shape. This is done using a homogenization approach developed for an array of resonators, and the resonance of an array is discussed when compared to that of a single resonator. The homogenization makes a parameter $\mathcal{B}$ to appear which determines unambiguously the resonance frequency of any neck. As expected, this parameter depends on the length and on the minimum opening of the neck, and it is shown to depend also on the surface of air inside the neck. Once these three geometrical parameters are known, $\mathcal{B}$ has an additional but weak dependence on the neck shape, with explicit bounds.

## I. INTRODUCTION

The vessels named "echea" are probably the first acoustic resonators. Described by Vitruvius in his "De Architectura", echea were used in ancient greek theaters for their acoustic properties [1] and later on in churches and mosques to improve the edifice sonority [2–4]. This resonator has been then studied in details by Helmholtz who was mainly interested in its musical properties [5], and nowadays, it is the most popular resonator for the acoustic waves, used to control and reduce the noise in ducts with flows [6] or used in the design of metasurfaces to realize sound collimators [7] or sound absorbers [8, 9].

Since Helmholtz's works, many studies have been devoted to this resonator and more or less sophisticated expressions of the resonance frequency have been proposed. Starting with Ingard [10], most of these studies use approximate modal methods and they aim to derive the so-called "added lengths" $e_{\text{ad}}$, which accounts for the effect of the evanescent field excited in the vicinity of the resonator neck, see *e.g.* [11]. This evanescent field, or near field, affects significantly the scattering properties of resonators with thin necks, the case of soda cans (with a neck reduced to a zero thickness diaphragm, $e = 0$ in Fig. 1(a)) being a limiting case. The added length enters in the expression of the wavenumbers $k_{\text{r}}$ at the resonances, with

$$\text{cotan} k_{\text{r}} d = k_{\text{r}} H \, \frac{e + e_{\text{ad}}}{h^-}, \tag{1}$$

whose popular expression for the lowest Helmholtz resonance with $k_{\text{r}} d \ll 1$ reads as

$$k_{\text{r}}^2 = \frac{h^-}{(e + e_{\text{ad}}) \mathcal{S}_{\text{c}}}, \tag{2}$$

written here in a two-dimensional configuration with $\mathcal{S}_{\text{c}} = dH$ the surface of the

cavity and $(e, h^-)$ the length and the minimum opening of the neck respectively (Fig. 1), see *e.g.* [12] and references herein. Modal methods have been shown to efficiently account for the near field effects for relatively simple geometries [10–13]. In this study, we are interested in exploring more complex neck shapes and we propose a model able to deal with such complexity. Beyond the fundamental interest of the study, adding extra degrees of freedom in the neck geometry may be of interest for practical applications including the use of these resonators in metamaterials [7–9].

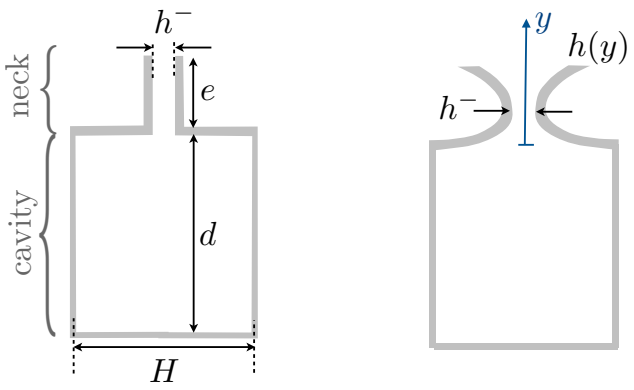


FIG. 1. (a) Simple geometry of the neck, for which (1) applies, (b) Complex geometry of the neck, for which (3) applies.

A typical question that we have in mind is the following: consider the four bottles in Fig. 2; can we predict their resonance frequencies or at least predict which ones give similar resonance frequencies ? To answer this question, we shall use a homogenization procedure able to encapsulate the effect of the necks in effective jump conditions. The homogenized model applies for an array of resonators producing a resonance frequency comparable to the resonance frequency of a single resonator. This is discussed in Section II where the resonances in the

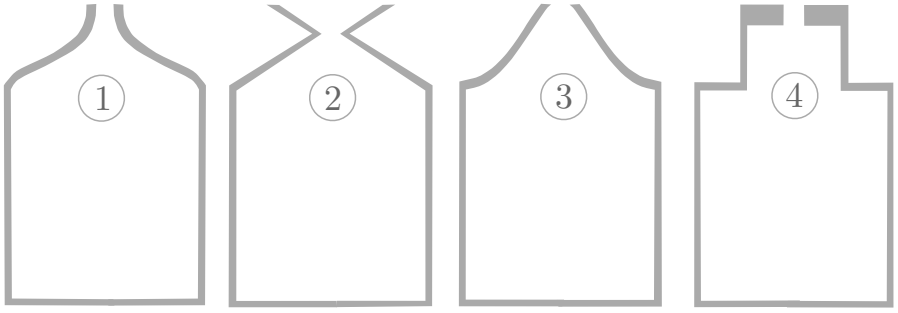


FIG. 2. Can we predict which bottles give similar resonance frequencies ?

homogenized model are found to be the solutions of the dispersion relation

$$\text{cotan} k_r d = k_r H \mathcal{B}, \tag{3}$$

where $\mathcal{B}$ depends on the shape of the neck only, and it is the unique quantity needed to determine $k_r$. The effective parameter $\mathcal{B}$ is obtained by solving a so-called elementary problem obtained in the homogenization procedure, which corresponds to the problem of a perfect fluid flowing in a duct obstructed by the neck. In this context, $\mathcal{B}$ measures the blockage of the flow due to the presence of this obstacle. Although $\mathcal{B}$ can be calculated numerically by solving the elementary problem, it makes sense to study its dependence with the geometrical parameters of the neck. This is the object of the section III; we show that $\mathcal{B}$ is essentially determined by three parameters being the length and the minimum opening of the neck, as expected from $(1)$, and in addition to the surface of air inside the neck. Once these three parameters are known, $\mathcal{B}$ has an additional but weak dependence on the neck shape. We give an explicit expression of $\mathcal{B}$ for a simple shape being formed by two parts with constant opening, a case which appears to be of particular interest, and we provide a procedure to get explicit bounds of $\mathcal{B}$ for an arbitrary neck shape. Finally, we inspect the validity of our homogenized model $(3)$ in Section IV in the light of comparison with direct

numerical calculations of the resonance frequencies.

## II. HELMHOLTZ RESONANCE IN THE HOMOGENIZED PROBLEM

### A. From a single resonator to an array of Helmholtz resonators

To begin with, we inspect the relation between the resonance of a single resonator and that of a periodic array of resonators, and to make the comparison possible, one has to define what we term resonance. For a single resonator, the resonances refer traditionally to the frequencies producing a peak of velocity in the neck. For an array of resonators, they are defined when the plane on the top of the necks is associated with a Dirichlet boundary condition for the acoustic pressure, see *e.g.* [14], which is consistent with the traditional conception. This condition is termed in-phase reflection in electromagnetism, and, transposed to acoustics, "in-phase" refers to no reflection phase shift of the acoustic velocity. For an open cavity ($h(y) = H$ and $e = 0$), it corresponds to the quarter wavelength criterion, with zero and maximum acoustic velocities at the extremities of the cavities.

To determine the link between the two criteria, we computed the resonance of a single resonator and that of arrays of resonators with different array spacings $s$; we used the finite element code XLiFE++ [15]. We considered a simple rectangular form of the necks as in Fig. 1(a) with $h^-/H = 0.1$, $e/H = 0.1$ and a cavity length set to $d/H = 1.5$. The variations of the pressure reflection coefficient $R$ are reported in Fig. 3 for $s/H = 1$, 3 and 7, and the pressure fields at the resonances defined as the in-phase reflection $\mathrm{Re}(R) = -1$ are shown in Fig. 4(a-c). For a single resonator, we computed the mean velocity, averaged in

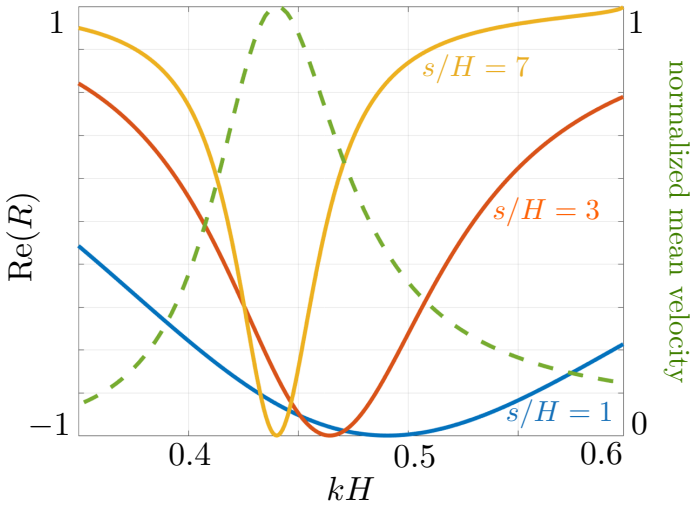


FIG. 3. Small shift in the resonance frequency for arrays of Helmholtz resonators with increasing relative spacings $s/H$; the resonances of the arrays are given by the in-phase condition $\mathrm{Re}(R) = -1$ (plain lines). The dotted line shows the variations of the velocity in the neck for a single resonator in free space (the mean velocity is normalized to its maximum value).

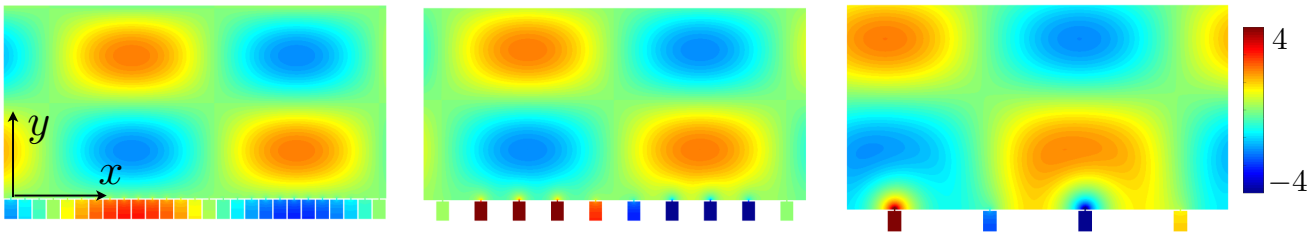


Arrays of resonators: (a) $s/H = 1$, (b) $s/H = 3$, (c) $s/H = 7$,

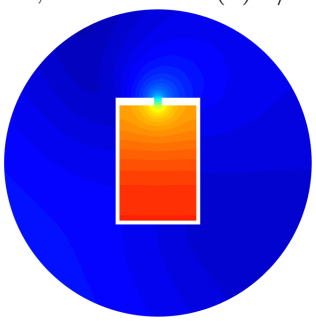

(d) Single resonator in free space

FIG. 4. Pressure fields at the resonances (a-c) for arrays of resonators with various spacings $s/H$; the incident plane wave of amplitude 1 is at oblique incidence $\theta = 30°$ , (d) for a single resonator in free space. Each resonator has dimensions $e/H = 0.1$, $h^-/H = 0.1$ and $d/H = 1.5$.

the volume of the neck. It is reported in Fig. 3 as a function of the frequency (dotted lines); the field at the frequency realizing the maximum velocity in the neck is shown in Fig. 4(d). In Fig. 3, we observe a small shift of the resonance frequencies of the arrays when increasing $s/H$ ($k_rH = 0.48$, 0.46 and 0.44) toward the frequency realizing the peak of velocity for the single resonator (at $k_rH = 0.44$). This result is quite intuitive; when they are close to each other, the resonators have interactions which result in a shift of their resonance frequency, and it turns out that this shift goes to higher frequencies. For larger spacings, these collective effects weaken and eventually, we recover the behavior of a single resonator. It is worth noting that this applies up to $s_c = 2\pi/k$ (at normal incidence); indeed, when $s > s_c$, higher diffracted waves appear which affect the resonance (see Appendix A). Finally, a small influence of the incidence angle on the resonance frequencies is observed for the arrays; this is not the case for a single resonator.

From what has been said above, the resonance frequency of an array of resonators does not coincide exactly with that of a single resonator and in fact, for a given shape of the resonator, the resonance of an array is not know precisely until the spacing has been defined. In the following, we shall consider the more compact array with $s = H$, which leads to a simpler effective model and allows us to focus on the effects of the neck only.

### B. Homogenization of an array of Helmholtz resonators

In the actual problem, the pressure $p(\mathbf{x})$ and velocity $\mathbf{u}(\mathbf{x})$ satisfy the Euler equations

$$\mathbf{u} = \boldsymbol{\nabla} p, \quad \text{div}\mathbf{u} + k^2 p = 0, \tag{4}$$

with $\mathbf{x} = (x, y)$, and the condition of vanishing normal velocity applies at each boundary between air and the rigid parts of the resonator. In the homogenized problem, the region of the cavities is simply replaced by air. The region of the necks is assumed to be small compared to that of the cavities and it is replaced by an interface across which jump conditions apply (Fig. 5). Specifically, the pressure field $p(y)$ in the homogenized problem satisfies

$$\begin{cases} \partial_{yy} p(y) + k^2 p(y) = 0, & -d < y < 0, \text{ and } y > e, \\ [\![p]\!] = H\mathcal{B}\, \overline{\partial_y p}, \quad [\![\partial_y p]\!] = -\dfrac{eH - \mathcal{S}_{\text{n}}}{H}\, k^2\, \overline{p}, & \\ \partial_y p(-d) = 0, & \end{cases} \tag{5}$$

where for any function $f(y)$, we have defined the jump $[\![f]\!] \equiv f(e) - f(0)$, and the mean value $\overline{f} \equiv \frac{1}{2}\,[f(0) + f(e)]$.

This is obtained owing to two simplifications in the actual problem. First and as previously said we consider a compact array with vanishing thickness of the cavity walls $s = H$. Next, we restricted ourselves to the case of waves at normal incidence on the array. The full calculation has to account, if $s \neq H$, for the thickness of the cavity wall, and, if oblique incidences are considered, for the rigid boundary condition on the cavity walls, see [16, 17] and Appendix A.

In $(5)$, a one dimensional wave equation applies for $-d < y < 0$ with Neumann boundary condition at $y = -d$. This is a classical result from the homogenization at the leading order, and it has been shown that the result holds true at the next order [16, 17]. In $(5)$, the jump conditions are a less classical result; we shall derive below these conditions for an incident wave at normal incidence.

The Helmholtz resonance being subwavelength, we have $ke, kH \ll 1$. For simplicity, we set $\varepsilon = H \ll 1$ with $k = O(1)$ and $e = O(H)$. Following [16, 17], we also use $d = O(1)$ and we define two expansions in the near and far fields of

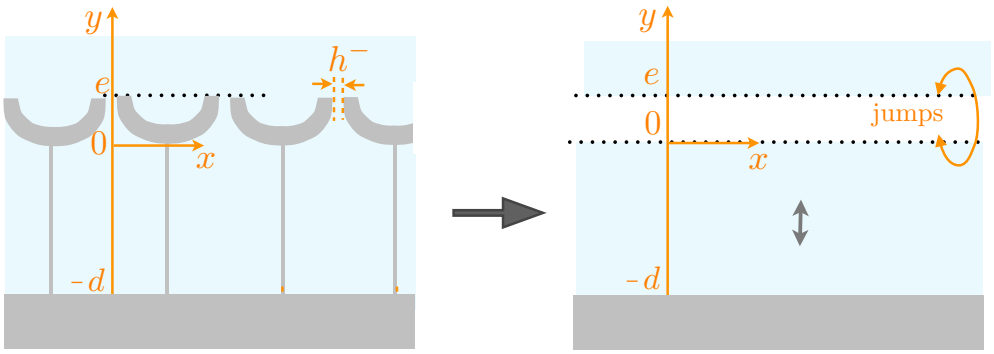


FIG. 5. From the actual problem to the homogenized problem. In the homogenized problem, the necks is replaced by a region across which jump conditions apply, Eqs. (5).

the necks, specifically

$$\begin{cases} p = p^0(y) + \varepsilon p^1(y) + \cdots, \quad \mathbf{u} = u_y^0(y)\mathbf{e}_y + \varepsilon u_y^1(y)\mathbf{e}_y + \cdots, & \text{in the far field,} \\ p = q^0(\boldsymbol{\xi}) + \varepsilon q^1(\boldsymbol{\xi}) + \cdots, \quad \mathbf{u} = \mathbf{v}^0(\boldsymbol{\xi}) + \varepsilon \mathbf{v}^1(\boldsymbol{\xi}) + \cdots, & \text{in the near field,} \end{cases} \tag{6}$$

with $\boldsymbol{\xi} = \mathbf{x}/\varepsilon$, and $\boldsymbol{\xi} = (\xi_x, \xi_y)$. In the far field, we used that $\partial/\partial_x = 0$ thus the problem is one dimensional along $y$. Obviously, this applies to the far field only; the near field, in the vicinity of the necks, contains the evanescent field which is two dimensional in $\boldsymbol{\xi}$ coordinates. Eventually, the near field is simply periodic with respect to $\xi_x$, of period unity in this rescaled coordinate. More specifically, the inner region is reduced to a strip $\mathsf{Y}_\infty = \{(-1/2, 1/2) \times (-\infty, \infty)\} \setminus S_\mathsf{n}$ where $S_\mathsf{n}$ is the region occupied by the rigid parts of the neck; we shall use also $\mathsf{Y} = \{(-1/2, 1/2) \times (-\xi_\mathsf{m}, \xi_\mathsf{m})\} \setminus S_\mathsf{n}$ ($\mathsf{Y}_\infty$ corresponds to $\mathsf{Y}$ for $\xi_\mathsf{m} \to +\infty$).

From a unique problem, we have built two problems, in the near and far fields, and we have to specify the boundary conditions for each one. The boundary conditions on the rigid parts of the necks apply to the near field solution, but boundary conditions are missing when $\xi_y \to \pm\infty$. Reversely, the radiation con-

ditions apply to the far field solution but there are missing boundary conditions when approaching the necks $y \to 0^{\pm}$. These missing boundary conditions are provided simultaneously by the matching conditions which read as

$$\begin{cases} p^0(0^{\pm}) = \lim\limits_{\xi_y \to \pm\infty} q^0(\boldsymbol{\xi}), & \mathbf{u}^0(0^{\pm}) = \lim\limits_{\xi_y \to \pm\infty} \mathbf{v}^0(\boldsymbol{\xi}), \\ p^1(0^{\pm}) = \lim\limits_{\xi_y \to \pm\infty} \left( q^1(\boldsymbol{\xi}) - \xi_y \dfrac{\partial p^0}{\partial y}(0^{\pm}) \right), & \mathbf{u}^1(0^{\pm}) = \lim\limits_{\xi_y \to \pm\infty} \left( \mathbf{v}^1(\boldsymbol{\xi}) - \xi_y \dfrac{\partial \mathbf{u}^0}{\partial y}(0^{\pm}) \right). \end{cases} \tag{7}$$

The above conditions tell us that the near and far fields have to coincide in some intermediate region, say at a distance $\sqrt{\varepsilon}$ of the necks, and there $y \sim \sqrt{\varepsilon} \to 0^{\pm}$ and $\xi_y = y/\varepsilon \to \pm\infty$. To derive the jump conditions which interrogate the far field solution for $y \to 0^{\pm}$, we shall use the expansions $(6)$ in $(4)$ with the differential operator $\nabla \to \mathbf{e}_y \partial_y$ in the far field and $\nabla \to (1/\varepsilon)\, \nabla_{\boldsymbol{\xi}}$ in the near field.

Let us start at the leading order. In the inner region, this leading order is in $1/\varepsilon$ in $(4)$. We get $\nabla_{\boldsymbol{\xi}} q^0 = 0$ from which $q^0$ is constant. The matching condition $(7)$ at the order 0 allows to conclude that $p^0(0^{\pm}) = q^0$ and thus, that $p^0$ is continuous at $y = 0$. Also, we get

$$\mathrm{div}_{\boldsymbol{\xi}} \mathbf{v}^0 = 0, \quad \lim_{\xi_y \to \pm\infty} \mathbf{v}^0 = u_y^0(0^{\pm})\, \mathbf{e}_y, \tag{8}$$

which shows that $\mathbf{v}^0$ is symmetric with respect to $\xi_x \in (-1/2, 1/2)$ in view of the symmetry of the problem; therefore, the periodic boundary conditions are equivalent to rigid boundary conditions $\mathbf{v}^0 \cdot \mathbf{n} = 0$. To end with the leading order, we integrate the relation $\mathrm{div}_{\boldsymbol{\xi}} \mathbf{v}^0 = 0$ over $\mathsf{Y}_{\infty}$; using the rigid boundary conditions on the neck boundary and at $\xi_x = \pm 1/2$, to get that $v_y^0(\xi_x, +\infty) = v_y^0(\xi_x, -\infty)$.

It is now sufficient to use the matching condition to conclude that $u_y^0$ is continuous at $y = 0$. The jump conditions at the leading order correspond to the usual continuity conditions of the pressure and of the normal velocity. In the present case, these conditions are clearly unsatisfactory since they ignore the effect of the neck.

To capture the effect of the evanescent field in the vicinity of the necks, we have to go to the next order. To do so, we consider the problem satisfied by $q^1$ in the near field region, with $\mathbf{v}^0 = \boldsymbol{\nabla}_{\boldsymbol{\xi}} q^1$ in $(8)$, and the boundary conditions $\mathbf{v}^0 \cdot \mathbf{n} = 0$ on the boundaries of the neck and at $\xi_x = \pm 1/2$. This problem is linear with respect to $\partial_y p_y^0(0) = u_y^0(0^{\pm})$ so that we can write

$$q^1(\boldsymbol{\xi}) = \partial_y p^0(0)\, \hat{q}(\boldsymbol{\xi}) + Q, \tag{9}$$

with $Q$ a constant and $\hat{q}(\boldsymbol{\xi})$ satisfying

$$\Delta_{\boldsymbol{\xi}} \hat{q} = 0, \quad \lim_{\xi_y \to \pm\infty} \boldsymbol{\nabla}_{\boldsymbol{\xi}} \hat{q} = \mathbf{e}_y, \tag{10}$$

and the same boundary conditions apply to $\hat{q}$ than to $q^1$. This is the elementary problem which will provide the parameter $\mathcal{B}$ involved in the jump conditions. Specifically, from $(10)$, $(\hat{q} - \xi_y)$ tends to constant values $\hat{\mathcal{B}}^{\pm}$ when $\xi_y \to \pm\infty$. Accordingly the field $\hat{q}$ reads as

$$\begin{cases} \hat{q}(\xi) = \xi_y + \hat{\mathcal{B}}^- + q^{\text{ev}}(\boldsymbol{\xi}),\ \xi_y < 0, \\ \hat{q}(\xi) = \xi_y + \hat{\mathcal{B}}^+ + q^{\text{ev}}(\boldsymbol{\xi}),\ \xi_y \geq 0, \end{cases} \tag{11}$$

where $q^{\text{ev}}$ is an evanescent field vanishing at $\xi_y \to \pm\infty$.

The jump of $p^1$ immediately follows owing to $(7)$ along with $(9)$ and $(11)$; we get $p^1(0^+) - p^1(0^-) = \hat{\mathcal{B}} \partial_y p^0(0)$, with $\hat{B} = \hat{B}^+ - \hat{B}^-$. To get the jump in $u_y^1$, we shall integrate over Y the relation $\text{div}_{\boldsymbol{\xi}} \mathbf{v}^1 + k^2 p^0(0) = 0$ (from $(4)$,

where we used that $q^0 = p^0(0)$ that we obtained at the leading order). Using the Neumann boundary conditions on the boundaries of the rigid parts and at $\xi_x = \pm 1/2$, we get $\int_{\mathsf{Y}} \mathsf{d}\boldsymbol{\xi}\ \mathrm{div}_{\boldsymbol{\xi}} \mathbf{v}^1 = v_y^1(\xi_x, +\xi_{\mathsf{m}}) - v_y^1(\xi_x, -\xi_{\mathsf{m}})$. We also have $\int_{\mathsf{Y}} \mathsf{d}\boldsymbol{\xi}\ p^0(0) = p^0(0)(2\xi_{\mathsf{m}} - \mathcal{S}_{\mathsf{n}}/H^2)$, where $\mathcal{S}_{\mathsf{n}}$ is the surface of the neck. With $\xi_{\mathsf{m}} \to +\infty$, it is sufficient to use the matching condition $(7)$ and the relation $\partial_y u_y^0 + k^2 p^0 = 0$, from $(4)$, to get $u_y^1(0^+) - u_y^1(0^-) = (\mathcal{S}_{\mathsf{n}}/H^2)\, k^2\, p^0(0)$.

The final jump conditions will be written after two last steps. Firstly, we shall express the jump conditions across an enlarged version of the interface; for the time being, they have been written across $y = 0^{\pm}$, thus reducing the regions of the necks to a zero thickness interface. Next, we shall write these jumps on a unique homogenized field $p^{\mathsf{h}}$ which admits the same expansion in $\varepsilon$ as $(p^0 + \varepsilon p^1)$, thus the same expansion as $p$, up to $O(\varepsilon^2)$. To do so, we use that $p^0(e) = p^0(0^+) + e\partial_y p^0(e) + O(e^2)$. With $e = O(\varepsilon)$, we get

$$\begin{aligned} \left[\!\left[p^0 + \varepsilon p^1\right]\!\right] &= e\partial_y p^0(e) + \varepsilon(p^1(0^+) - p^1(0^-)) + O(\varepsilon^2) \\ &= (e + H\hat{\mathcal{B}})\ \overline{\partial_y p^0} + O(\varepsilon^2) \\ &= (e + H\hat{\mathcal{B}})\ \overline{\partial_y (p^0 + \varepsilon p^1)} + O(\varepsilon^2), \end{aligned} \tag{12}$$

since $p^0(0^+) - p^0(0^-) = 0$ and $\overline{\partial_y p^0} = \partial_y p^0(e) + O(\varepsilon)$ (and the same with $\partial_y p^0(0)$). Doing the same for $(u_y^0 + \varepsilon u_y^1)$, it is easy to see that $p^{\mathsf{h}}$ satisfying (i) $\partial_{yy} p^{\mathsf{h}} + k^2 p^{\mathsf{h}} = 0$ outside the enlarged interface $y \in (0, e)$, and (ii) the jumps across the enlarged interface $\left[\!\left[p^{\mathsf{h}}\right]\!\right] = (e + H\hat{\mathcal{B}})\ \overline{\partial_y p^{\mathsf{h}}}$ and $\left[\!\left[\partial_y p^{\mathsf{h}}\right]\!\right] = -(e - \mathcal{S}_{\mathsf{n}}/H) k^2 \overline{p^{\mathsf{h}}}$, admits the same expansion as $(p^0 + \varepsilon p^1)$ up to $O(\varepsilon^2)$, thus the same expansion of $p$ up to $O(\varepsilon^2)$. We recover $(5)$ with $\mathcal{B} = e/H + \hat{\mathcal{B}}$.

Note that we can derive jump conditions involving other value of $\mathcal{B}_a = a/H + \hat{\mathcal{B}}$

across interfaces enlarged to a thickness $a = O(e)$ (this excludes values of $a$ of the order of $d$). The resulting models are all equivalent up to $O(\varepsilon^2)$ but may slightly differ in terms of accuracy, see [18**?** ].

### C. Resonance frequency in the homogenized problem

The homogenized problem $(5)$ is one-dimensional, and it is easy to solve it for an incident plane wave along $y$. The solution reads as

$$\begin{cases} p(y) = e^{-ik(y-e)} + Re^{ik(y-e)}, \ y > e, \\ \\ p(y) = A \ \cos k(y+d), \qquad -d < y < 0, \end{cases} \tag{13}$$

where the boundary condition $\partial_y p(-d) = 0$ has been accounted for. The reflection coefficient $R$ and the constant $A$ are determined by the jump conditions in $(5)$, which allows us to determine the wavenumbers $k_{\mathrm{r}}$ at the resonances defined by $R = -1$, solutions of the dispersion relation

$$\mathcal{B} k_{\mathrm{r}} H \tan k_{\mathrm{r}} d + \frac{k_{\mathrm{r}}^2}{4} \mathcal{B} \left( eH - \mathcal{S}_{\mathrm{n}} \right) = 1. \tag{14}$$

Owing to the fact that the contribution in $k_{\mathrm{r}}^2$ in the right hand side term is small compared to 1 ($k_{\mathrm{r}}^2 eH = O(\varepsilon^2)$), we get cotan$k_{\mathrm{r}} d = k_{\mathrm{r}} H \, \mathcal{B}$ according to $(3)$.

## III. THE BLOCKAGE COEFFICIENT IN THE ELEMENTARY PROBLEM

From $(3)$, it is sufficient to compute $\mathcal{B}$ to get the resonance frequency, and we shall see in the following section that this is true. Thus, it makes sense to inspect in some details the variation of $\mathcal{B}$ with the neck shapes, in order to draw the tendencies that may help us to design the necks for a given purpose. To that aim, we shall first see some qualitative properties of $\mathcal{B}$. Then, we shall consider in

details the case of a simple neck shape composed of two-stepwise constant parts, hereafter termed two-step neck, for which an excellent approximate expression of $\mathcal{B}$ is available. Besides, it appears that such simple neck, with 2 degrees of freedom (in addition to $h^-/H$ and $e/H$), describe the whole accessible space for $\mathcal{B}$. This means that a neck with any complicated shape profile has the same resonance frequency (because the same $\mathcal{B}$) than a two-step neck, in fact the same as a collection of them. Based on this fact, we provide bounds for $\mathcal{B}$ for an arbitrary neck shape.

### A. Some qualitative properties of $\mathcal{B}$

The elementary problem $(10)$ which provides $\mathcal{B} = \hat{\mathcal{B}} + e/H$ is a static problem, which corresponds to a perfect fluid flowing in a duct obstructed by the neck (Fig. 6). In general, this problem has to be solved numerically, but we can already anticipate which neck geometries will produce high or low $\mathcal{B}$ values. With $\hat{p}$ the velocity potential, the constant $\hat{\mathcal{B}}$, often termed blockage coefficient, measures the deviation of the streamlines with respect to the straight lines that we would have in an empty duct. As a first remark, the flow being reversible, the neck can be upturned without affecting the value of $\mathcal{B}$, a fact of interest when one considers Helmholtz resonators with necks inserted partially or totally inside the cavity [13, 19, 20].

Next, increasing $e/H$ or decreasing $h^-/H$ produces an increasing blockage of the flow, whence an increase in $\mathcal{B}$. In the absence of neck $\hat{\mathcal{B}} = 0$ and it is positive otherwise; this can be already seen from $(1)$ with $\mathcal{B} \geq e/H$.

Finally, the regions where the fluid is at rest are of particular interest. Indeed, they behave as rigid parts, being delimited by a streamline with vanishing normal

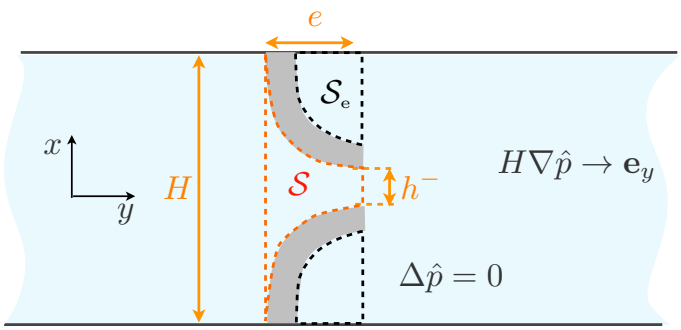


FIG. 6. Elementary problem in actual scales, with $\hat{p}(\mathbf{x}) = \hat{q}(\boldsymbol{\xi})$ the velocity potential associated to a flow in a duct obstructed by an obstacle. The obstacle is characterized by its length $e/H$ and the minimum relative opening $h^-/H = \alpha^-$. The perfect fluid flows through a region of surface $\mathcal{S} = \varphi_\mathrm{n}\, eH$ (inner region) within the neck. The outer region $\mathcal{S}_\mathrm{e}$ roughly corresponds to a region where the flow is at rest.

velocity, by definition. As such, starting from a neck producing such regions, we can build a family of necks with the same $\mathcal{B}$ by replacing these regions, partially or totally, by rigid parts. We expect the fluid to be at rest in the region of surface $\mathcal{S}_\mathrm{e}$ in Fig. 6; it is the outer region of the neck through which the flow cannot pass and inside which it will not enter deeply. We have checked this property on $\mathcal{B}$, and illustrations will be given in the forthcoming section.

From what has been said below, we expect that only the inner surface $\mathcal{S}$ of air in the neck, corresponding to the region where the fluid can flow, influences the value of $\mathcal{B}$. From now on, and to avoid heavy notations, we define

$$\varphi_\mathrm{n} = \frac{\mathcal{S}}{eH}, \quad \alpha^- = \frac{h^-}{H}, \tag{15}$$

being respectively the inner filling fraction of air and the relative minimum opening of the neck (whence by construction $0 \leq \alpha^- \leq 1$ and $\alpha^- \leq \varphi_\mathrm{n} \leq 1$).

### B. The case of two-step neck shapes

We term two-step neck shape a neck made of two rectangular parts, with

$$\begin{cases} h(y) = \alpha^+ H,\ 0 \leq y < \beta e, \\ h(y) = \alpha^- H,\ \beta e < y \leq e, \end{cases} \tag{16}$$

see the inset of Fig. 7. Extending the approximate expression of $\mathcal{B}$ given in [18] for a one step rectangular neck, it appears that $\mathcal{B}$ is accurately described by the expression

$$\mathcal{B} = \frac{e}{H}\left[\frac{(1-\beta)}{\alpha^-} + \frac{\beta}{\alpha^+}\right] - \frac{1}{\pi}\log\left(\sin\frac{\pi\alpha^-}{2}\,\sin\frac{\pi\alpha^-}{2\alpha^+}\,\sin\frac{\pi\alpha^+}{2}\right). \tag{17}$$

In addition to $e/H$ and $\alpha^-$, this family of necks has two other degrees of freedom being $\alpha^+ \in (\alpha^-, 1)$ and $\beta \in (0, 1)$ the relative opening and relative thickness of the largest part of the neck. Next, the inner fraction of air in the neck is given by

$$\varphi_{\mathsf{n}} = \alpha^-(1-\beta) + \alpha^+\beta. \tag{18}$$

There are two contributions in the expression of $\mathcal{B}$, $(17)$. The first contribution, proportional to $e/H$ is related to the propagation of the low frequency wave; it would be obtained by approximate modal methods only accounting for the propagating wave and as such, appears as a simple extension of $(1)$ with $e_{\mathsf{ad}} = 0$. We term this contribution the propagation contribution. The second contribution in $\log$ is well known and it is exact in the case of a single diaphragm with zero thickness (the derivation using techniques of complex variables can be found in [21]). It is for instance the unique contribution to $\mathcal{B}$ for a soda can resonator; in this case, with $e = 0$, there is no propagation contribution and with $\alpha^+ = \alpha^-$ the diaphragm only produces a near field contribution (with

$\mathcal{B} = -2/\pi \log \sin(\pi\alpha^-/2)$). In $(17)$, we assume that the expression of the near field contribution holds true at each discontinuity in the neck cross section; next using the reversibility of the flow, the contribution is written in order that either an expansion or a contraction produces an increase in $\mathcal{B}$ (thus, with an argument in each sine being smaller than $\pi/2$).

Inspecting the variations of $\mathcal{B}$ with $\alpha^+$ and $\beta$ reveals that $\mathcal{B}$ can take any value between two extreme curves parametrized by $\varphi_n$: $\mathcal{B}_M$ corresponding to $\alpha^+ = 1$ (a single step shape) and $\mathcal{B}_m$ corresponding to $\beta = 1$ (a diaphragm with opening $\alpha^-$ staked to a single step). These two extrema are given by

$$\begin{cases} \mathcal{B}_m = \dfrac{e}{H}\dfrac{1}{\varphi_n} - \dfrac{1}{\pi}\log\left[\sin\left(\dfrac{\pi\alpha^-}{2}\right)\,\sin\left(\dfrac{\pi\varphi_n}{2}\right)\,\sin\left(\dfrac{\pi\alpha^-}{2\varphi_n}\right)\right], \\ \mathcal{B}_M = \dfrac{e}{H}\left[1 + \dfrac{1-\varphi_n}{\alpha^-}\right] - \dfrac{2}{\pi}\log\sin\left(\dfrac{\pi\alpha^-}{2}\right), \end{cases} \tag{19}$$

and they coincide at their minimum and maximum for $\varphi_n = 1$ and $\varphi_n = \alpha^-$ respectively, with

$$\begin{cases} \min(\mathcal{B}_M) = \min(\mathcal{B}_m) = \dfrac{e}{H} - \dfrac{2}{\pi}\log\left(\sin\dfrac{\pi\alpha^-}{2}\right) \\ \max(\mathcal{B}_M) = \max(\mathcal{B}_m) = \dfrac{e}{h^-} - \dfrac{2}{\pi}\log\left(\sin\dfrac{\pi\alpha^-}{2}\right), \end{cases} \tag{20}$$

and these bounds are given once $\alpha^- = h^-/H$ and $e/H$ have been chosen.

To illustrate what has been said above, Fig. 7 reports the variations of $\mathcal{B}$ computed numerically by solving the elementary problem, $(10)$-$(11)$ (open symbols). We considered fixed values of $\alpha^- = h^-/H = 0.1$ and $e/H = 0.45$ and varied continuously $\varphi_n$. For comparison, we reported $\mathcal{B}$ predicted by $(17)$ (plain lines). Expectedly, $\mathcal{B}$ describes the interior of a wing shape region, bounded by $(19)$ and with extreme values equal to 1.63 and 5.71 in agreement with $(20)$, and as we

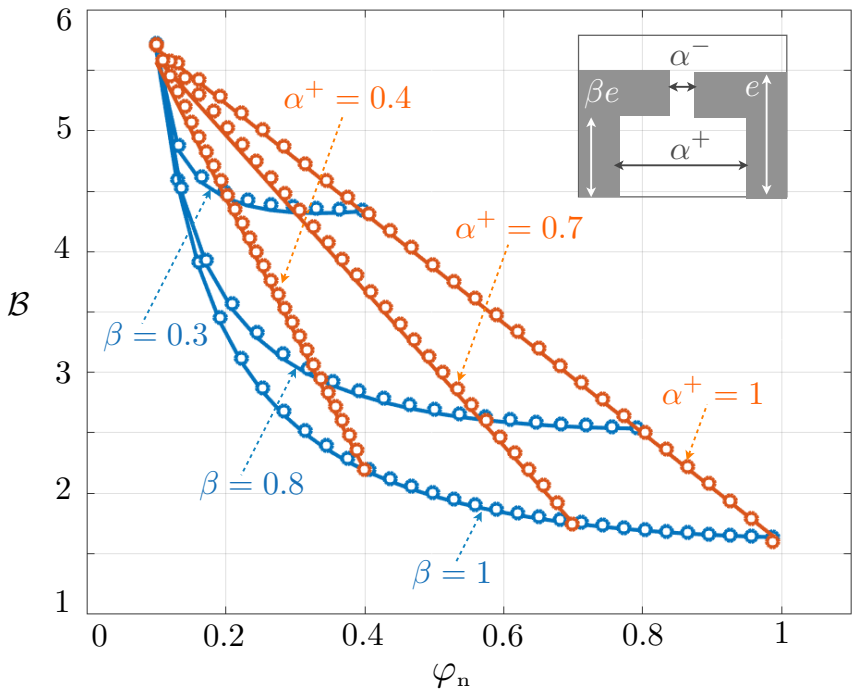


FIG. 7. Variation of $\mathcal{B}$ for fixed values of $\alpha^- = 0.1$ and $e/H = 0.45$ as a function of $\varphi_{\rm n}$, (18), for a two-step neck shape (shown in the inset). $\mathcal{B}$ describes the interior of a wing for varying $\alpha^+$ and $\beta$ according to (17) (plain lines); the open symbols show the actual values of $\mathcal{B}$ from the resolution of the elementary problem (10)-(11). The wing shape is bounded by $\mathcal{B}_{\rm M}$ for $\alpha^+ = 1$ and $\mathcal{B}_{\rm m}$ for $\beta = 1$, (19).

announced, the accuracy of (17) is excellent. Note that once $(\alpha^-, e/H, \varphi_{\rm n})$ are given, $\mathcal{B}$ is determined and it corresponds to a unique neck shape, from (17)-(18). This is of importance if we have in mind the inverse problem in which we want to determine the neck able to produce a given resonance frequency with geometrical constraints (the constraints are for instance the values of $e/h$ and $\alpha^-$ that we keep constant).

We shall see in the following section that the bounds (19) and (20) seem to hold for any neck shapes being described by an arbitrary neck shape $h(y)$ once $(\alpha^-, e/H)$ are given, and we shall propose a procedure to get more precise bounds.

### C. Arbitrary neck shape

We now move on the case of necks with arbitrary shapes being described by $h(y)$ and the corresponding local opening and inner surface

$$\alpha(y) = \frac{h(y)}{H}, \quad \mathcal{S} = \int_0^e h(y)\, dy. \tag{21}$$

For a two-step neck shape, we identified in $(17)$ the propagation contribution and the near field contribution. Our guess is that the value of $\mathcal{B}$ for an arbitrary neck shape reads as

$$\mathcal{B} = \int_0^e \frac{dy}{h(y)} - \frac{1}{\pi} \log\left( F(\alpha)\ \sin\frac{\pi\alpha(e)}{2} \right). \tag{22}$$

In the above expression, the integral is the continuous version of the propagation contribution in $(17)$. In the second term, which encapsulates the near field contribution, we accounted for the diaphragm effect at the end of the neck which is the rule more than the exception (if it is not the case, $\alpha(e) = 1$ and this contribution vanishes). Next, we ask to the function $F(\alpha)$ to account for all the near field effects in the neck for $0 \leq y \leq e$. Obviously, this contribution cannot be evaluated in an arbitrary case, and this is why $\mathcal{B}$ has to be calculated numerically in general by solving $(10)$, with $(11)$. However, it is possible to find bounds for $F(\alpha)$ if we admit that any discontinuity in the neck between $\alpha(y)$ and $\alpha(y + \delta y)$ produces a contribution of the form

$$\cdots \sin\frac{\pi\alpha(y)}{2\alpha(y+\delta y)} \cdots, \tag{23}$$

which is written here for an expansion (the case of a constriction involves $\pi\alpha(y+\delta y)/2\alpha(y)$ in the argument of the sine). In fact the easiest way to find such bounds, which does not mean that it is the most precise, is as follows. We

discretize the interval $(0, e)$ into $N$ parts with $\delta y = e/N$, producing a set of $\{\alpha_i\}_{i=0,\dots,N}$ with $\alpha_i = \alpha(i\delta y)$ (and $\alpha_0 = 1$ at $y = 0$ by construction). Doing so, we can construct $F_N(\alpha)$ such that

$$F_N(\alpha) = \prod_{i=0}^{N} \sin \frac{\pi \alpha_i}{2\alpha_{i+1}}, \tag{24}$$

written here for a series of expansions with $\alpha_{i+1} > \alpha_i$; in the more general case, one choose the ratio of $\min(\alpha_i, \alpha_{i+1})$ and $\max(\alpha_i, \alpha_{i+1})$ for each $i$. It is worth noting that an alternative choice would be to fix $\delta\alpha$ with a resulting variable $\delta y$.

In any case, $F_\infty > F_N$ which means that using $F = F_\infty$ in $(22)$ defines a lower bound for $\mathcal{B}$. Indeed, for a continuous function $\alpha(y)$, $F_\infty = 1$ since $\alpha_i/\alpha_{i+1} \to 1$ when $N \to \infty$. Thus, in a general case, only the discontinuous parts of $\alpha(y)$ will be captured in this limit. However, evanescent waves are excited in the physical problem even for a continuous profile and this cannot be estimated within the present procedure.

An upper bound is more difficult to define and other constructions of the $F_N$ could be chosen depending on the considered shape. As the simplest rule, we consider the maximum of $F_N$ when varying $N$. By construction, we obviously find that $N = 1$ maximizes $F_N$ if $\alpha(e) = \alpha^-$, otherwise the maximum is found for $N$ equals few unities.

For several neck shapes, we calculated $\mathcal{B}_N$ using $F = F_N$ in $(22)$ varying $N$ and the exact value of $\mathcal{B}$ solving the elementary problem $(10)$-$(11)$. Typical variations of $\mathcal{B}_N$ are reported in Fig. 8 in plain lines, with extreme values bounding, as expected, the actual value of $\mathcal{B}$ (in dotted line).

Doing so for two families of shapes, we obtain the representation of the Fig. 9 (the parametrization of these profiles are given in Appendix B). As for the

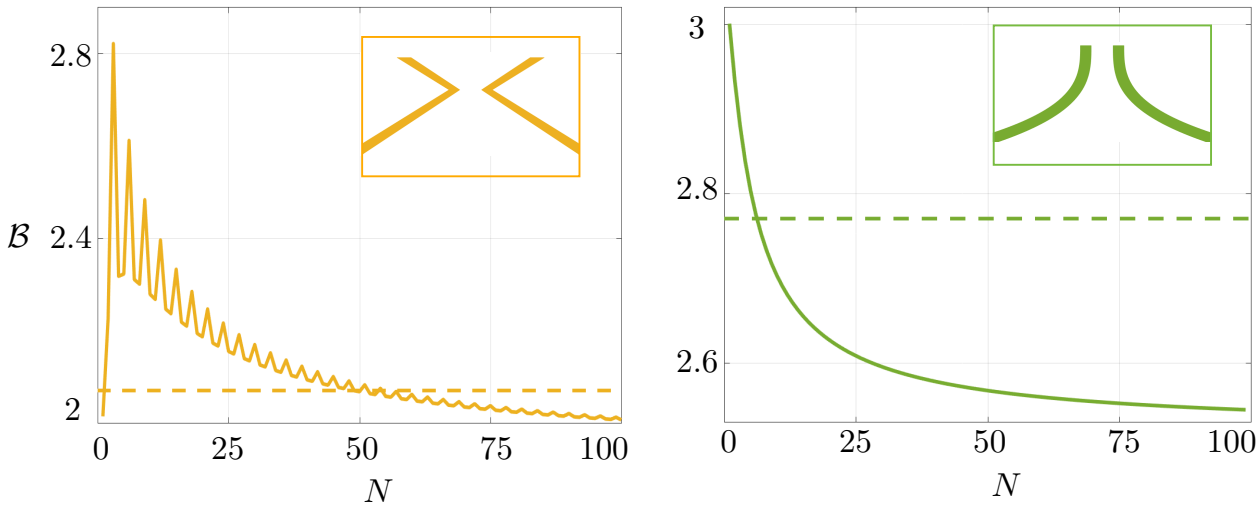


FIG. 8. Variations of $\mathcal{B}_N$ using $F = F_N$, (24) in (22) for two necks (the neck shape are shown in the inset, see Appendix B). The dotted lines show the actual value of $\mathcal{B}$ from the resolution of the elementary problem (10)-(11).

two-step necks, we have imposed the same values of $\alpha^- = h^-/H$ and of $e/H$. These calculations seem to show that $\mathcal{B}$ lies inside the wing region defined by the two-step necks.

## IV. VALIDATION OF THE HOMOGENIZED MODEL FOR THE HELMHOLTZ RESONANCE

Having drawn the tendencies and the variations of $\mathcal{B}$ as a function of the three main geometrical parameters $(h^-/H, e/H, \varphi_n)$ and as a function of the shape, it remains to be seen whether the Eq. (3) is able to predict the frequency of the Helmholtz resonance.

### A. Upturned and filled necks

We start with the properties announced for $\mathcal{B}$: we said that (i) the region of the neck through which the fluid cannot flow (in the elementary problem) can

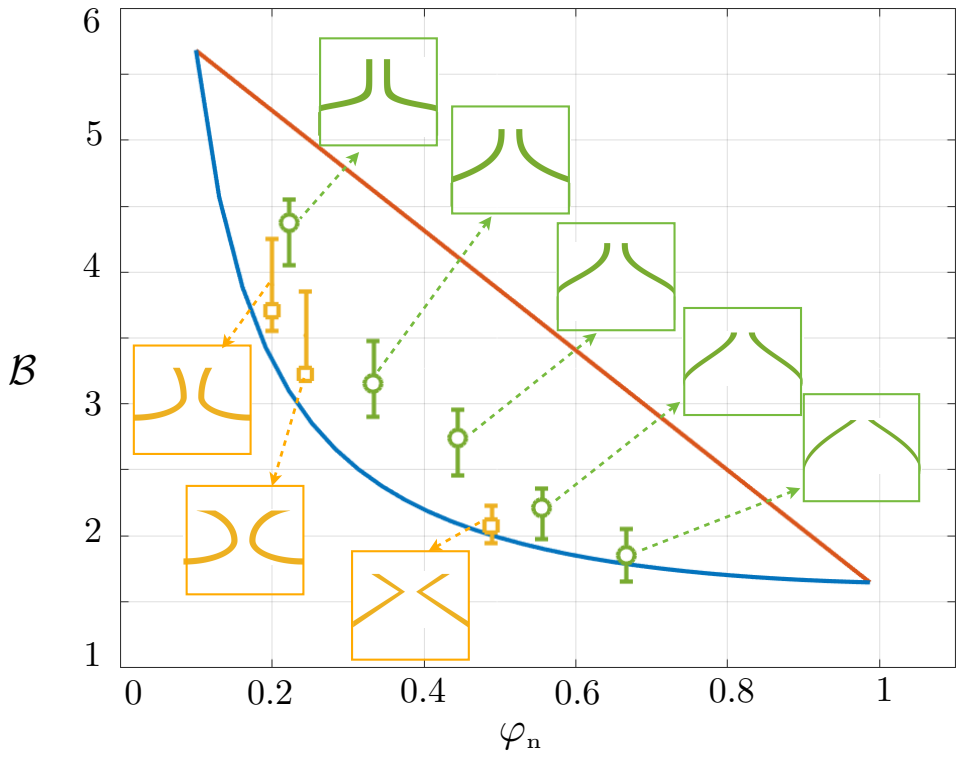


FIG. 9. Examples of $\mathcal{B}$ values for continuously varying neck shapes calculated by solving the elementary problems (10)-(11) (open symbols, the insets show the corresponding shapes, all with $\alpha^- = 0.1$ and $e/H = 0.45$); the bars around each symbol show the bounds of $\mathcal{B}_N$, from the procedure illustrated in Fig. 8. The plain lines are the bounds for $\mathcal{B}$, (19).

be filled with rigid material without affecting $\mathcal{B}$, whence without affecting the resonance, and (ii) the neck can be upturned without affecting the resonance frequency, Fig. 10.

We have computed $\mathcal{B}$ for the two shapes of the necks reported in the insets (a) and (c) in Fig. 11. Evidently, $\mathcal{B}$ is found to be the same for a given neck and its upturned version. Next, for the one step neck in Fig. 11(a), we found $\mathcal{B} = 5.67$ for an outer part of the neck being filled with air and $\mathcal{B} = 5.71$ for an outer part of the neck being filled with a rigid material. For the continuously varying neck shape in Fig. 11(c), we found $\mathcal{B} = 2.88$ and $\mathcal{B} = 2.93$ respectively. As expected, the values are close to each other in both cases.

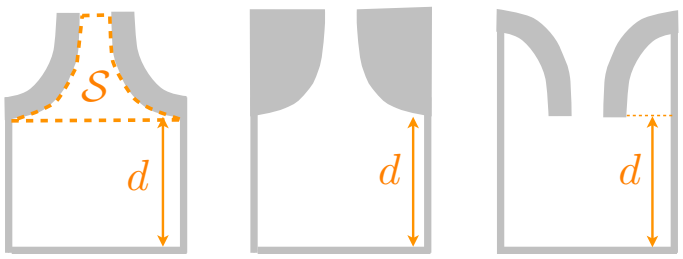


FIG. 10. Helmholtz resonators with necks with the same shape $h(y)$ and (a) a finite wall thickness leaving an outer region filled with air, (b) an outer region filled with rigid material (c) an upturned neck.

Next, we computed numerically the resonance curves for these necks surmounting a cavity of length $d/H = 2$; results are shown in Fig. 11(b).We observe that the resonance frequencies of cavities surmounted by the 3 necks are very close, as expected. Besides, these resonance frequencies are in good agreement with $(3)$ which gives for (a) $k_r H \simeq 0.28$ and for (c) $k_r H \simeq 0.37$.

### B. Resonance frequencies in the actual and homogenized problems

We computed numerically the reflection curve as a function of $kH$ for two-step necks producing the values of $\mathcal{B}$ given in Fig. 7. For each curve, we stored the resonance frequency $k_r H$ realizing in-phase reflection, $\mathrm{Re}(R) = -1$. The results are reported in Fig. 12 together with the homogenized prediction $(3)$ using the estimate $(17)$ for $\mathcal{B}$. We considered the neck surmounting a cavity with length $d/H = 2$ and $d/H = 4$. The agreement is in general good, which confirms the accuracy of the homogenized model. However, it is visible that it is much better for the largest cavity length $d/H = 4$. The relative disagreement between the actual resonance frequencies and the homogenized prediction for $d/H = 2$ is attributable to two effects which are difficult to separate. On the

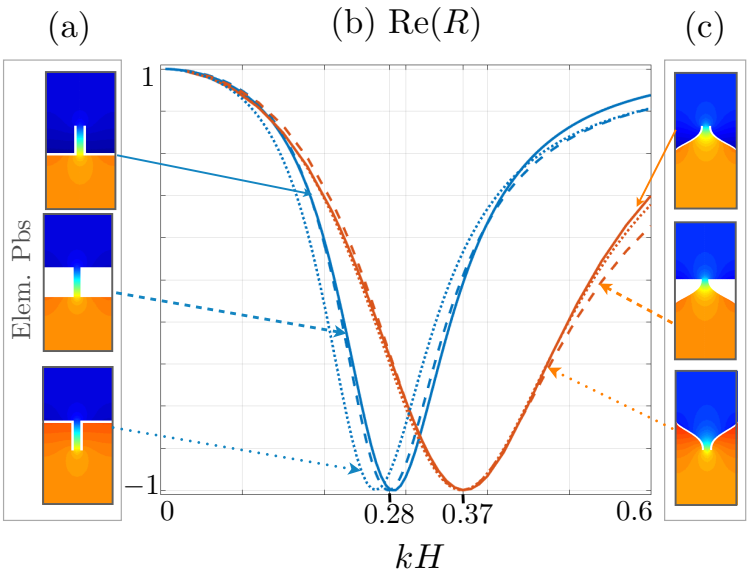


FIG. 11. (a) and (c) Fields of the velocity potential in the elementary problem (10) from which $\mathcal{B}$ is deduced, for a neck with an outer part filled with air (top panel), filled with a rigid material (center panel) and upturned (bottom panel); two neck shapes are considered. (b) Real parts of the reflection coefficients calculated numerically. The resonance frequencies are in good agreement with (3) which gives for (a) $k_{\rm r}H \simeq 0.28$, and for (c) $k_{\rm r}H \simeq 0.37$.

one hand, a smaller cavity depth $d$ produces a higher resonance frequency $k_{\rm r}H$ which eventually exits from the range of validity of the homogenization since we assumed $kH \ll 1$. On the other hand, we have assumed that propagation effect occurs in the cavity, with $d \gg H, e$, and this penalizes also values of $d/H$ of the order than 1.

The same representation is used in Fig. 13 for the necks with continuously varying shape shown in Fig. 9. We reported the resonance frequencies $k_{\rm r}H$ computed numerically (open symbols) and the bars being deduced from (3) with the values of $\mathcal{B}_N$ reported in Fig. 9 (from (22) with (24)). The conclusion is the same as for the two-step shapes with an overall good agreement, and the procedure to get approximate values of $\mathcal{B}$ and thus to get the resonance frequency of an arbitrary neck shape appears to be satisfactory. As expected, all

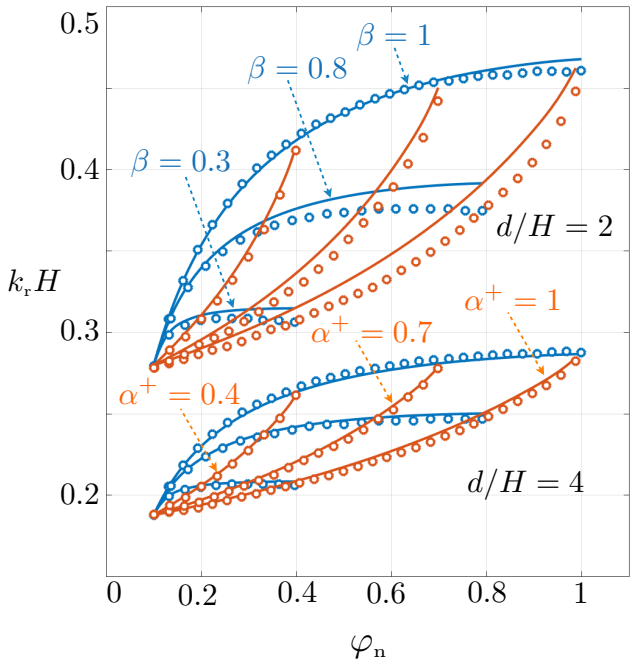


FIG. 12. Resonance frequencies as a function of $\varphi_n$ for two-step necks (same representation as in Fig. 7) surmounting a cavity with $d/H = 2$ and $d/H = 4$. Open symbols show the resonance frequencies calculated numerically and plain lines reports the homogenized prediction (3) using $\mathcal{B}$ in (17).

the resonance frequencies are bounded by the resonance frequencies given by (3) with $(\mathcal{B}_m, \mathcal{B}_M)$ in (19) (plain lines).

Finally, the range of accessible $k_r H$ values for varying shape decreases when $d$ increases, with a limit given by the asymptotic behavior $k_r = \pi/(2d)$ for large $d$ value.

## V. CONCLUDING REMARKS

We have presented a homogenization procedure able to describe the scattering property of arrays of Helmholtz resonators with arbitrary neck shape. In the resulting homogenized problem, the resonances are known unambiguously once a coefficient $\mathcal{B}$ has been calculated, (3). This coefficient is the blockage coefficient

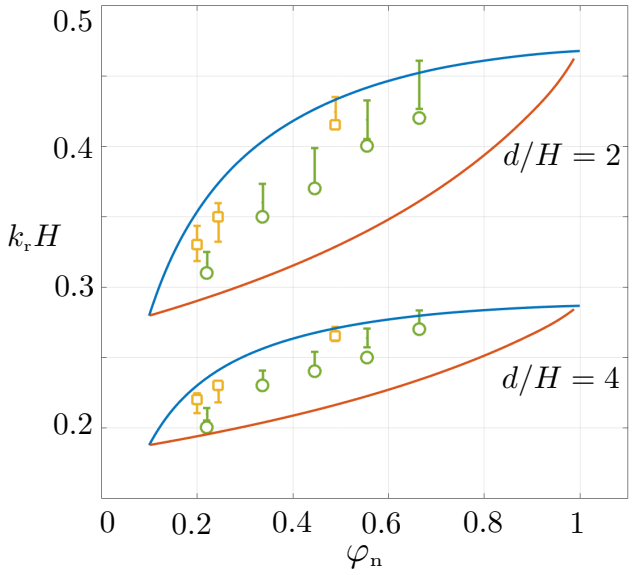


FIG. 13. Same representation as in Fig. 12 for continuous varying neck shapes (the necks are the same as in Fig. 9). Open symbols show the resonance frequencies calculated numerically and bars the bounds deduced from $\mathcal{B}_N$ (see Fig. 9) in (3). The plain lines report the bounds of $k_{\rm r}H$ for $\mathcal{B}$ in (19).

of the simple potential flow problem of a fluid flowing in a duct obstructed by the resonator neck.

If a direct problem is thought where a given neck is considered, we have shown that the three geometrical parameters $(e/H, \alpha^-, \varphi_{\rm n})$ already provide bounds $(\mathcal{B}_{\rm m}, \mathcal{B}_{\rm M})$ of $\mathcal{B}$, (19), therefore they provide bounds for the resonance frequencies $k_{\rm r}H$, with (19) in (3). Then, more precise bounds are possible considering the variations of $\mathcal{B}_N$ in the procedure presented in Sec. III.

If an inverse problem is thought where a neck producing a given resonance frequency is looked for, the family of the two-step necks is of particular interest. Indeed, this family has the huge advantage to have a closed form of $\mathcal{B}$, (17), which implies few degrees of freedom. Moreover, focusing on this family is not restrictive since it seems that any neck shape has a two-step alter ego

producing the same resonances, see Fig. 14 with the illustrative examples of our study. Notably, we illustrated that $\mathcal{B}$ has still some flexibility when geometrical constraints are imposed. We have considered the two most usual constraints on the compactness of the array given by $(e+d)$ and on the minimum opening $h^-$ which controls the main source of viscous dissipation (and this later effect can be unwanted for acoustic purpose or desired for application to perfect absorption devices). Incidentally, these shapes are also easy to manufactured compared to their continuously varying counterparts.

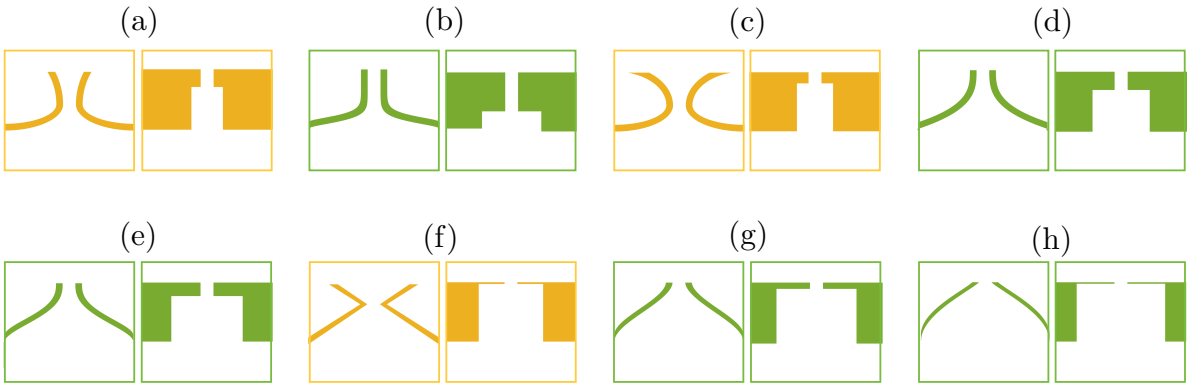


FIG. 14. Equivalence between a smoothly varying profile and a two-step shape with the same $(e/H, \alpha^-, \varphi_n)$ and $\mathcal{B}$. For each couple (a) to (h), on the left a profile from Fig. 9 and on the right the corresponding two-step shape providing the same resonance frequencies. (a) $\varphi_n = 0.20$, (b) $\varphi_n = 0.22$, (c) $\varphi_n = 0.24$, (d) $\varphi_n = 0.33$, (e) $\varphi_n = 0.44$, (f) $\varphi_n = 0.49$, (g) $\varphi_n = 0.56$, (h) $\varphi_n = 0.67$ (for $\mathcal{B}$, see Figs. 9).

We end these concluding remarks by giving the response to our question in Fig. 2, which is basically the kind of response given in Fig. 14. In Fig. 2, the necks have the same $e/H = 0.45$, $\alpha^- = 0.1$ and $\varphi_n = 0.2$ and they differ only by their shapes under these constraints. Next, computing $\mathcal{B}$ gives $\mathcal{B} \simeq 2.7$ for the profiles 1 and 4 and $\mathcal{B} \simeq 2.1$ for the profiles 2 and 3, which allows us to

conclude.

## ACKNOWLEDGMENTS

We thank the anonymous referee for his very helpful comments and suggestions. The authors acknowledge the financial support of the french Mission Interdisciplainare du Centre National de la Recherche Scientifique (MI/CNRS) under grant INFYNITI/PomS.

## Appendix A: Resonance curves in the homogenized problem

In Fig. 3, we reported resonance curves calculated numerically. Then only the resonance frequencies deduced from these numerical curves and that given by $(3)$ in the homogenized problems were compared, and we restricted ourselves to the case $s/H = 1$. For a sake of completeness, we report in this appendix comparisons of the entire resonance curves. When the thickness of the wall does

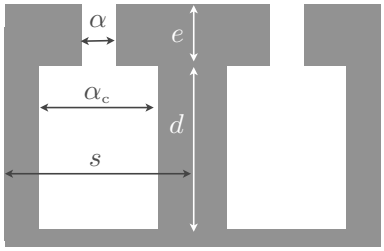


FIG. 15. Array of Helmholtz resonators with non vanishing thickness of the cavity walls ($s/H > 1$).

not vanish ($s/H > 1$) and at oblique incidence, the jump conditions read

$$[\![p]\!] = s\mathcal{B}\,\overline{v}, \quad [\![v]\!] = -s\mathcal{C}\,\frac{\partial^2 \overline{p}}{\partial x^2} - e\varphi_{\text{n}} k^2 \overline{p}, \tag{A1}$$

with $[\![v]\!] = v(x,e) - v(x,0)$ the jump of the normal component of the acoustic velocity (along $y$), but now $v(x,e) = \partial_y p(x,e)$ and $v(0) = (\alpha_{\text{c}}/s)\partial_y p(x,0)$, see

[16]. This is because the region of the cavities is now replaced by an effective anisotropic medium with the acoustic velocity $\mathbf{u} = (u, v)$ with $u = 0$ and $v = (\alpha/s)\partial_y p$; this tell us that the propagation is allowed along $y$ only, as expected. In addition, we have div$\mathbf{u} + k^2(\alpha/s)p = 0$, from which the propagation is described by the wave equation $\partial_{yy}p + k^2 p = 0$ (with the same wavenumber as in air). Thus, in $(\mathrm{A1})$, $s$ appears since $[\![v]\!]$ and $\overline{v}$ depends on this $\alpha_{\mathrm{c}}/s$. Next, $\mathcal{B}$ is affected since the flow in the elementary problem $(10)$, see also $(11)$, now takes place in a duct of varying section: it is of width $\alpha_{\mathrm{c}}/s$ in the inner region $\xi_y < 0$ and of width 1 for $\xi_y > e/s$. As in $(5)$ and according to $(15)$, the parameter $\varphi_{\mathrm{n}}$ is defined by

$$\varphi_{\mathrm{n}} = \frac{es - \mathcal{S}_{\mathrm{n}}}{es} \tag{A2}$$

being the filling fraction of air in the neck (for a simple neck shape as in Fig. 15, $\varphi_{\mathrm{n}} = \alpha/s$). Finally, $\mathcal{C}$ is a new parameter in $(\mathrm{A1})$ which is involved in the jump conditions only if $p$ depends on $x$ that is for oblique incidence. For the one-step neck in Fig. 15, we have good estimates of $(\mathcal{B}, \mathcal{C})$ in the forms

$$\begin{cases} \mathcal{B} = \dfrac{e}{\alpha} - \dfrac{1}{\pi}\log\left(\sin\dfrac{\pi\alpha}{2}\sin\dfrac{\pi\alpha}{2\alpha_{\mathrm{c}}}\right), \\ \mathcal{C} = \dfrac{e\alpha}{s^2} - \dfrac{\pi}{4}\left(\dfrac{\alpha}{s}\right)^2. \end{cases} \tag{A3}$$

In the following, we considered $H = 1$, $\alpha = 0.1$, $\alpha_{\mathrm{c}} = 1$, $e = 0.1$ and $s = 1, 3, 7$. Computing $\mathcal{B}$ and $\mathcal{C}$ by means of the elementary problems, we find the parameters entering in $(\mathrm{A1})$: $s\mathcal{B}$ = 2.5 7.7 19.8 and $s\mathcal{C} = 0.0018$, 0.0007, 0.0003 respectively. Our estimates $(\mathrm{A3})$ give $s\mathcal{B} = 2.4$, 7.6 and 19.6, and $s\mathcal{C}$= 0.0020, 0.0007, 0.0003. Finally, $e\varphi_{\mathrm{n}}$ = 0.0100 0.0033 0.0014. The same coefficients apply for any cavity depth $d$.

For an oblique incidence $\theta$, we look for a solution of the form

$$\begin{cases} p(y) = e^{ik_x x}\left(e^{-ik_y(y-e)} + Re^{ik_y(y-e)}\right), \; y > e, \\ \\ p(y) = A\, e^{ik_x x}\, \cos k(y+d), \qquad\qquad -d < y < 0, \end{cases} \tag{A4}$$

with $k_x = k\cos\theta$, $k_y = k\sin\theta$. The reflection coefficient in the homogenized problem then reads as

$$\begin{cases} \qquad R = -\dfrac{Z}{Z^*}, \\ \text{with} \quad Z = z_1 y_1 - z_2 y_2, \\ \text{and} \quad \begin{array}{ll} z_1 = 1 + i\dfrac{\mathcal{B}}{2}\, k_x s, & z_2 = ik_x + \dfrac{1}{2}\left(\mathcal{C}k_y^2 s - \dfrac{\alpha_c}{s}k^2 e\right), \\ y_1 = \dfrac{k\alpha_c}{s}\tan(kd)\dfrac{1}{2} - \left(\mathcal{C}k_y^2 s - \dfrac{\alpha_c}{s}k^2 e\right), & y_2 = 1 - \dfrac{\mathcal{B}}{2}k\alpha_c \tan(kd). \end{array} \end{cases} \tag{A5}$$

Fig. 16 report the variations of $R$ (real part) already shown in Fig. 3 obtained numerically (open symbols in Fig.16) and given by the homogenized prediction $(\mathrm{A5})$ (plain lines). We considered incidence angles $\theta = 0$, 30 and 60° and cavity depths $d = 1.5$ and $d = 6$ (resulting in $k_r H \simeq 0.44$ and $k_r H \simeq 0.19$ respectively). For $d = 6$, the agreement is good for the three spacing and for any incidence. For $d = 1.5$, the agreement remains relatively good but fails for $\theta = 60°$ and $s/H = 7$; in this case, the mode -1 realizing $k_{-1}s = 2\pi/(1+\sin\theta)$ appears for $k < k_{-1} = 0.48$ at $\theta = 60°$ which makes the homogenized prediction unreliable.

From the inspection of these results, the homogenized model is unexpectedly robust and the reason remains to be clarified. Indeed, the small parameter in the asymptotic analysis is now $ks$. Thus for $s/H = 7$, the prediction is correct while $ks$ has largely overcame 1. It would be for instance helpful to conduct the homogenization at higher orders, and determine the scaling of the higher order

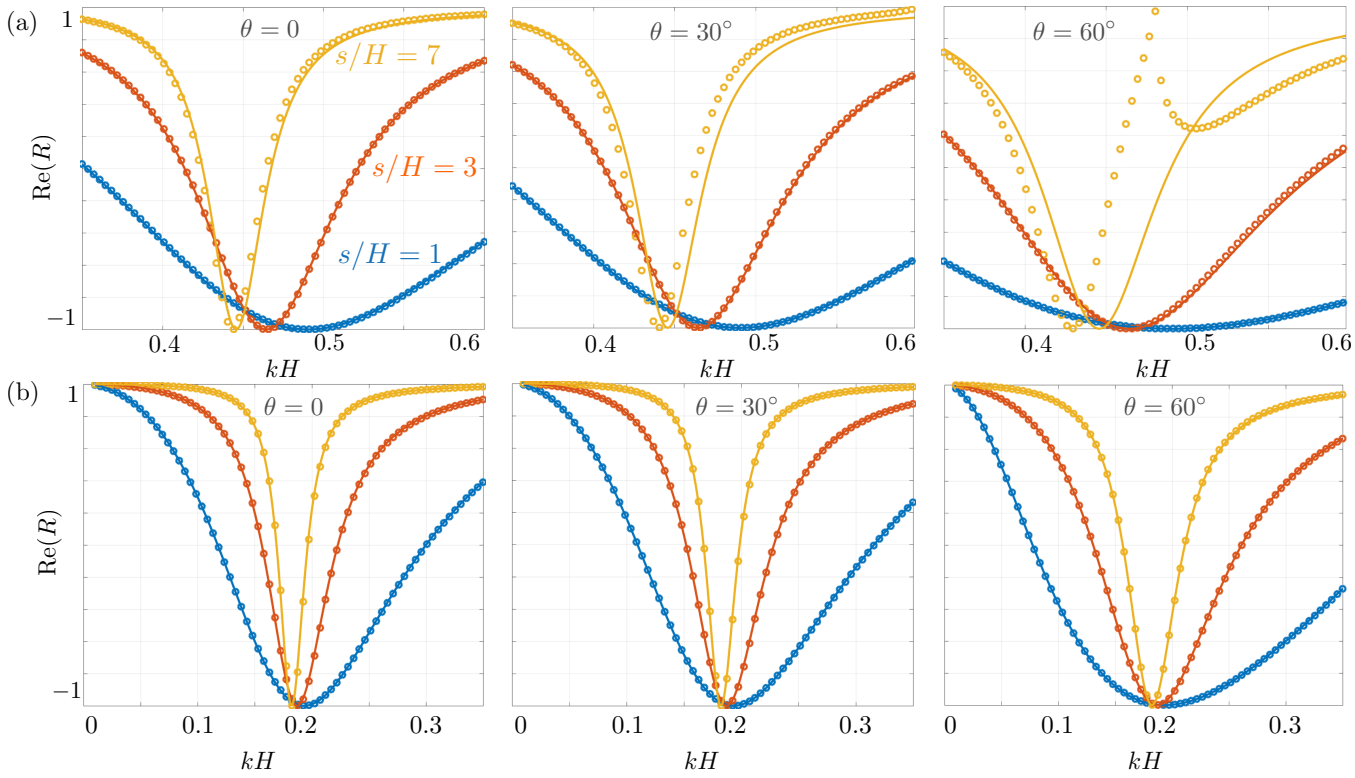


FIG. 16. Comparison of the resonance curves from numerics (symbols) and in the homogenized model, Eq. (A5). (a) for the same configuration as in Fig. 3, $d = 1.5$ and (b) for the same geometry of the necks and $d = 6$.

effective parameters, say $\mathcal{B}_i$ for $i > 1$ (with $\mathcal{B} = \mathcal{B}_1$); if $\mathcal{B}_i$ is sufficiently small in a sense which remains to determine, we could have $\varepsilon^i \mathcal{B}_i \ll \varepsilon \mathcal{B}$ for $\varepsilon = ks > 1$.

## Appendix B: Continuously varying shape - choice of the parametrization

The first family of shapes are parametrized by two parameters $(a, b)$

$$\begin{aligned} y &= 0.45 - t, \\ x &= A\left[1 - \left(\frac{t}{A}\right)^b\right]^a, \end{aligned} \tag{B1}$$

and

$$\begin{cases} t \in (0.40, 0), \ A = 0.40, \\ t \in (0, 0.45), \ A = 0.45. \end{cases} \tag{B2}$$

In practice, $(a, b)$ are of the order of unity (the circles in Fig. 9).

The second family of shapes are parametrized by four parameters $(A, T, a, b)$ with

$$\begin{aligned} y &= t_1 - t, \\ x &= A\left[1 - \left(\frac{t}{T}\right)^b\right]^a, \end{aligned} \tag{B3}$$

and

$$\begin{cases} t \in (0, t_1), & A = 0.45,\ T = t_1, \\ t \in (t_1 - 0.45, 0), & A = 0.45,\ T = t_1 - t_2, \\ t \in (t_1 - 0.05, 0), & A = 0.40,\ T = t_1 - 0.05, \\ t \in (0, t_1 - 0.45), & A = 0.40,\ T = t_1 - t_2 + 0.45. \end{cases} \tag{B4}$$

In practice, $(A, T, a, b)$ are of the order of unity (the squares in Fig. 9).

---


[1] S. Polychronopoulos, D. Kougias, P. Polykarpou, and D. Skarlatos, Acta Acustica united with Acustica **99**, 64 (2013).

[2] T. Zakinthinos and D. Skarlatos, Applied Acoustics **68**, 1307 (2007).

[3] J.-C. Valière, B. Palazzo-Bertholon, J.-D. Polack, and P. Carvalho, Acta Acustica united with Acustica **99**, 70 (2013).

[4] M. R. Ismail, Frontiers of architectural research **2**, 30 (2013).

[5] H. Helmholtz and A. J. Ellis, "On the sensations of tone, as a physiological basis for the theory of music," (1886).

[6] W. Bi, V. Pagneux, D. Lafarge, and Y. Aurégan, The Journal of the Acoustical Society of America **122**, 280 (2007).

[7] L. Quan, F. Qian, X. Liu, X. Gong, and P. A. Johnson, Physical Review B **92**, 104105 (2015).

[8] N. Jiménez, W. Huang, V. Romero-García, V. Pagneux, and J.-P. Groby, Applied Physics Letters **109**, 121902 (2016).

[9] V. Romero-García, G. Theocharis, O. Richoux, A. Merkel, V. Tournat, and V. Pagneux, Scientific reports **6** (2016).

[10] U. Ingard, The Journal of the acoustical society of America **25**, 1037 (1953).

[11] J. Kergomard and A. Garcia, Journal of Sound and Vibration **114**, 465 (1987).

[12] R. Chanaud, Journal of Sound and Vibration **178**, 337 (1994).

[13] A. Selamet and I. Lee, The Journal of the Acoustical Society of America **113**, 1975 (2003).

[14] L. Quan, X. Zhong, X. Liu, X. Gong, and P. A. Johnson, Nature communications **5**, 3188 (2014).

[15] http://uma.ensta paristech.fr/soft/XLiFE++/, (2017).

[16] A. Maurel, J.-J. Marigo, J.-F. Mercier, and K. Pham, unpublished (2017).

[17] J.-J. Marigo and A. Maurel, SIAM Journal on Applied Mathematics **77**, 721 (2017).

[18] J.-J. Marigo and A. Maurel, The Journal of the Acoustical Society of America **140**, 260 (2016).

[19] Z. Kang and Z. Ji, Journal of Sound and vibration **310**, 782 (2008).

[20] P. Chaitanya and M. Munjal, Applied Acoustics **72**, 65 (2011).

[21] P. M. Morse and K. U. Ingard, *Theoretical acoustics* (Princeton university press, 1968).